Available online at www.sciencedirect.com
ScienceDirect
Journal of the Franklin Institute 348 (2011) 999–1012
Journal of The Franklin Institute
www.elsevier.com/locate/jfranklin

Hybrid position/force control of a flexible parallel manipulator ☆

M. Madani, M. Moallem*

Mechatronics Systems Engineering, Simon Fraser University, Surrey, BC, Canada

Received 6 December 2007; received in revised form 13 March 2011; accepted 14 March 2011
Available online 21 March 2011

Abstract

In this paper, simultaneous position/force control of a closed-chain planar manipulator with the last link flexible is studied when the manipulator is in contact with an environment. The proposed manipulator consists of a flexible link connected to three rigid linkages whichare optimized for kinematic and force manipulability in the region of interest. The flexible link is modeled as a series of rigid links connected by virtual torsion springs. A hybrid position/force control algorithm is developed and implemented on the manipulator. Experimental results are presented to verify the performance of the controller.

1. Introduction

Robotic devices have been used in industrial applications in the past but are finding new applications in areas such as service operations [1] and medical robotics [2]. The use of robots in medical procedures and rehabilitation is an emerging area due to its potential to facilitate medical procedures by utilizing accurate sensors and actuators integrated with modern electronics and embedded computers [2,3]. The design and construction of a robot manipulator equipped with a flexible link presented in this paper is motivated by the increasing demand in the field of *medical robotics* to automate surgical procedures involving operations with structurally flexible tools. Simultaneous position and force control of the

☆This research was supported in part by grants from the Natural Sciences and Engineering Research Council (NSERC) of Canada and the Simon Fraser University Startup Fund.
*Corresponding author. Tel.: +1 778 782 8156.
E-mail address: mmoallem@sfu.ca (M. Moallem).

0016-0032/$32.00
doi:10.1016/j.jfranklin.2011.03.005

flexible manipulator is of interest in robot-assisted needle insertion [4,5] and soft tissue cutting operations, where the tools such as a slender needle may be deflected during the procedure. For example, in robot-assisted brachytherapy, low-dose radioactive seeds are implanted in specific parts of an organ containing cancerous tumours. The success depends greatly on the precision of positioning the implanted radioactive seeds. Another application is cutting soft tissue using a surgical blade. In these applications, control of the tip position and the force exerted by the tool is desirable. The reason why using a flexible manipulator is more favorable in force control problems is its compliance with the environment which avoids generation of large impulsive forces when the robot contacts the environment.

In this study, we utilize a parallel planar manipulator for investigating simultaneous position/force control. Physical parameters such as link lengths of the manipulator are determined using a numerical optimization algorithm based on a global iso-conditioning index (GII) that maximizes a performance index over a region of interest in the manipulator's workspace. Modeling flexible-link manipulators has been extensively studied in the literature, for instance, by Cannon et al. [6] who used assumed-mode discretization. Cho et al. [7] used cubic splines to approximate the kinematics of the flexible link under bending conditions. Computational approaches were introduced in [9] for flexible multi-body systems that can be applied to robots with flexible links.

In advanced robotic applications, a robot manipulator is required to interact compliantly with its environment. In such cases, not only precise positioning control is required, but also the amount of force exerted by the manipulator on the environment must be carefully controlled. Simultaneous force and position control for constrained robot systems has been an active area of research [8,10–15]. Due to the complexity of the kinematic and dynamic equations, absence of the inverse kinematic equation, and presence of kinematic redundancy in the flexible manipulator, most well-known control schemes are not capable of satisfying the control objectives. This poses a challenge on the available control schemes such as hybrid position/force control (or hybrid control for brevity) and impedance control. The objective of this work is to design a feedback control law so that the position and the force exerted by robot's end-effector follow desired trajectories in the presence of structural flexibility.

2. Description of the manipulator system

The flexible manipulator comprises the closed-chain kinematic system depicted in Figs. 1 and 2 where all the links and joints are made of rigid material except the last link L_{10} which is flexible. The manipulator consists of eight passive and four active revolute joints connected by 10 rigid links to form three linkages. The manipulator can move just in the XY plane. Links L_9 and L_{10} are clamped together by a six axis force/torque sensor located in the middle of L_9. A six axis force/torque sensor is located in the middle of L_9. Four DC servo motors are responsible for providing appropriate torques for the active joints A, A', C, and C', which are attached to the base to decrease the inertia of the moving parts. The geometry of the parallel manipulator is considered to be symmetric to achieve better performance as discussed in [16]. The overall degrees of freedom are three, which correspond to two translational and one rotational degree of manipulability at the end effector (T). The orientation of the end effector is denoted by ζ which is defined as the counter-clockwise angle between non-deflected L_{10} and L_0. The optimum physical parameters of the manipulator such as link lengths are obtained to achieve the best possible kinematic and dynamic conditioning in a certain part of the workspace by maximizing GII [17] over a desired region of the manipulator's workspace.

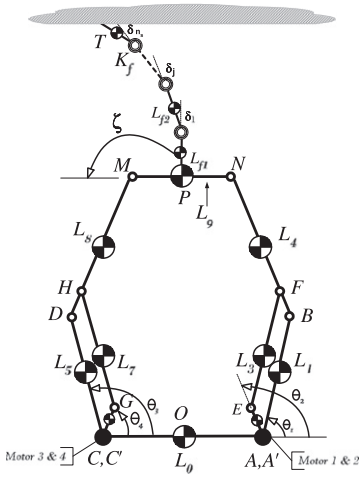

Fig. 1. Proposed flexible manipulator constrained to the environment.

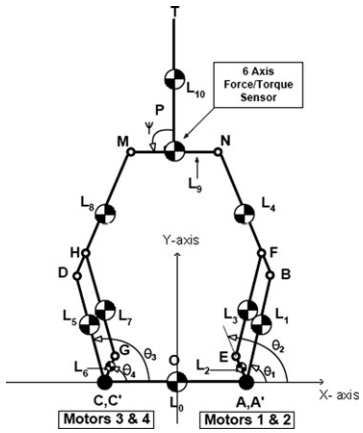

Fig. 2. Another view of the parallel manipulator in stretched condition.

Yoshikawa [8] introduced a new approach for modeling a flexible beam which is suitable for real-time control and is utilized in this work. In this approach, the flexible beam is modeled using some rigid links connected by virtual torsional springs as illustrated in Fig. 1. Assuming small deflections, Zaki and Elmaraghy [18] obtained the appropriate spring stiffness coefficients by matching the end point deflection of a lumped spring-mass to that of a cantilevered flexible beam which yields

$$K_f = \frac{3EI}{L_{sl}} \frac{n_s(n_s+1)(2n_s+1)}{6(n_s+1)^2} \tag{1}$$

where E denotes modulus of elasticity, I is the flexible beam moment of inertia, L_{sl} represents length of each sub-link used in the flexible link which is $L_{flexibleLink}/(n_s+1)$, and n_s is the number of springs used in the modeling of the flexible link. The constructed

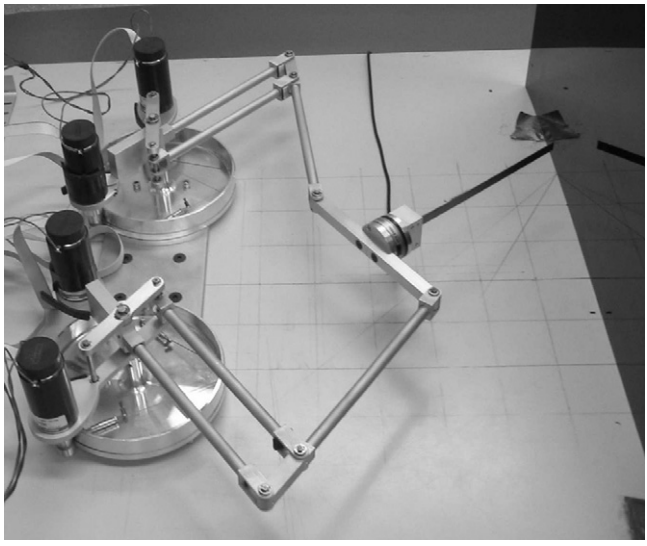

Fig. 3. Constructed flexible manipulator in contact with a rigid environment.

flexible manipulator is shown in Fig. 3. Like other discretization methods, the more rigid links and virtual joints used in the model, the more accurate approximation is achieved.

2.1. Forward and inverse kinematics of the manipulator

The forward kinematic equation, $p=f(q)$, maps the configuration space Q into the task space P ($f:\mathbb{R}^n\to\mathbb{R}^m$) where n and m represent the dimensions of the two spaces, respectively. In Fig. 1, given the vector of joint angles $q=[\theta_i\ \delta_j]^T$, where $\theta_i(i=1,\ldots,4)$ represents the active joints and δ_j ($j=1,\ldots,n_s$) is the discretized beam deflection vector, the kinematic equations are given by

$$x_T = x_P - \frac{L_{sl}}{2}\sin(\gamma) - \sum_{j=1}^{n_s}\frac{L_{sl}}{2}\sin(\gamma+\delta_j) \tag{2}$$

$$y_T = y_P + \frac{L_{sl}}{2}\cos(\gamma) + \sum_{j=1}^{n_s}\frac{L_{sl}}{2}\cos(\gamma+\delta_j) \tag{3}$$

$$\zeta = \frac{\pi}{2} - \arctan\left(\frac{\alpha}{\beta}\right) \tag{4}$$

where L_{sl} is the length of each small sub-rigid link in the flexible beam (thus each rotational spring is connected to two beams of length $L_{sl}/2$ each), $\gamma=\pi-\zeta$, and α and β are the x- and y-coordinates of point P in Figs. 1 and 2. Using trigonometric relationships one can obtain the following:

$$x_P = (x_M + x_N)/2$$

$$y_P = (y_M + y_N)/2$$

$$x_M = -\frac{L_0}{2} + L_1 c_3 + L_4 c_4$$

$$y_M = L_1 s_3 + L_4 s_4 \tag{5}$$

$$x_N = \frac{L_0}{2} + L_1 c_1 + L_4 c_2$$

$$y_N = L_1 s_1 + L_4 s_2 \tag{6}$$

$$(L_9)^2 = (x_M - x_N)^2 + (y_M - y_N)^2 \tag{7}$$

$$\alpha = L_1(c_1 + c_3) + L_4(c_2 + c_4)$$

$$\beta = L_0 + L_1(s_1 + s_3) + L_4(s_2 + s_4)$$

$$\gamma = \pi - \zeta$$

$$c_i = \cos(\theta_i), \quad s_i = \sin(\theta_i)$$

In the above equations, L_i ($i = 1,\ldots,9$) is the length of link i in the main rigid chain. It is important to note that in the kinematics of the rigid manipulator ζ might be considered as one of the task-space variables, while Fig. 1 shows that this is not to be the case in the flexible manipulator.

Fig. 1 shows that for a given position of the tip of the flexible manipulator, there is an infinite number of solutions for the active joint angles and the flexible-link deflection modes. This means that for a given tip position (p), the active joint angles depend on not only the position of the tip, but also on the amount of force that is being exerted by the flexible manipulator on the environment (λ), i.e., $\theta = g(p, \lambda)$.

The linear velocity of the end-effector can be obtained by taking derivative of Eqs. (2) and (3) with respect to time. The Jacobian matrix of the flexible manipulator, J_f is defined as

$$\dot{p} = J_{f(n\times m)}\dot{q} \tag{8}$$

In the rest of this paper $J_{f(n\times m)}$ is indicated by J.

2.2. Dynamics of the system

The Lagrangian formulation is employed to obtain the system dynamics which results in

$$M(q)\ddot{q} + C(q,\dot{q})\dot{q} + Kq = \begin{bmatrix} \tau \\ 0 \end{bmatrix} \tag{9}$$

which can be re-expressed as

$$\tau = M_{11}(q)\ddot{\theta} + M_{12}(q)\ddot{\delta} + C_1(q,\dot{q}) \tag{10}$$

$$0 = M_{21}(q)\ddot{\theta} + M_{22}(q)\ddot{\delta} + C_2(q,\dot{q}) + K\delta \tag{11}$$

where M_{ij} ($i,j = 1,\ldots,n$) represent sub-matrices of the mass matrix M, C_1 and C_2 represent centrifugal and Coriolis terms, K represents the diagonal stiffness matrix $K(q) \in \mathbb{R}^{n\times n}$ with K_f being the spring constant of the torsional springs.

Interaction of the manipulator with an environment can be formulated using constraint equations $\Phi_i : Q \mapsto X$, where

$$\Phi_i(q_1, q_2, \ldots, q_n) = 0, \quad i = 1, \ldots, k \tag{12}$$

Imposing k independent holonomic constraints reduces the number of degrees of freedom of the system to $(n-k)$ which implies a reduced set of generalized coordinates, $\tilde{q}^T = [\tilde{q_1}, \ldots, \tilde{q_{n-k}}]$ that can be used to describe the constrained motion. Holonomic constraints can be obtained by taking the first and second derivatives of Eq. (12) with respect to time. Thus we have

$$A(q)\dot{q} = 0 \tag{13}$$

$$A(q)\ddot{q} + \dot{A}(q)\dot{q} = 0 \tag{14}$$

where

$$A(q) = \frac{\partial \Phi_i(q)}{\partial q} \in \mathbb{R}^{k \times n} \tag{15}$$

Thus the constrained equation of motion can be obtained as

$$M(q)\ddot{q} + C(q, \dot{q})\dot{q} + Kq + A^T(q)\lambda = \tau \tag{16}$$

where $\lambda \in \mathbb{R}^k$ is a vector of *Lagrange multipliers*, and can be interpreted as the magnitude of the related force vector normal to each constraint [19] and can be obtained by simultaneously solving Eqs. (14) and (16) which results in

$$\lambda = (AM^{-1}A^T)(AM^{-1}(\tau - C\dot{q} - Kq) + \dot{A}\dot{q}). \tag{17}$$

3. Force and position control

Let us consider an application involving cutting tissue (environment) using a structurally flexible tool and a surgical blade. This can be simulated by sliding the tip of the flexible manipulator along the environment while exerting specific forces on the environment. As depicted in Fig. 1, we assume that the flexible beam is always in contact with the environment defined geometrically by an algebraic constraint given by Eq. (13). Further, the flexible beam is modeled using two rigid sub-links connected by one spring moving in the XY plane. The control objective is to slide the tip of the flexible beam along the X-axis on the environment according to a pre-planned trajectory profile while regulating the exerted force normal to the constraint (along the Y-axis) according to a certain force profile. Due to the fact that control variables belong to two orthogonal subspaces, a decoupling control scheme such as hybrid position/force control can be utilized [20].

In a classical hybrid control scheme, the task space is decomposed into two complementary orthogonal subspaces using compliant selection matrices S and $S^{\perp}$, where S is an $m \times m$ diagonal and idempotent matrix with the elements defined as either being 1, for position control, and 0 for force control. Also, $S^{\perp}$ is an $m \times m$ complementary matrix of S whose elements are 1, for force control, and 0 for position control. In the hybrid position/force control scheme shown in Fig. 4, the following relationships are satisfied

$$p_{es} = SJq_e \tag{18}$$

$$q_{es} = J^{-1}p_{es} \tag{19}$$

$$\tau_{es^{\perp}} = S^{\perp}J^T\lambda_e \tag{20}$$

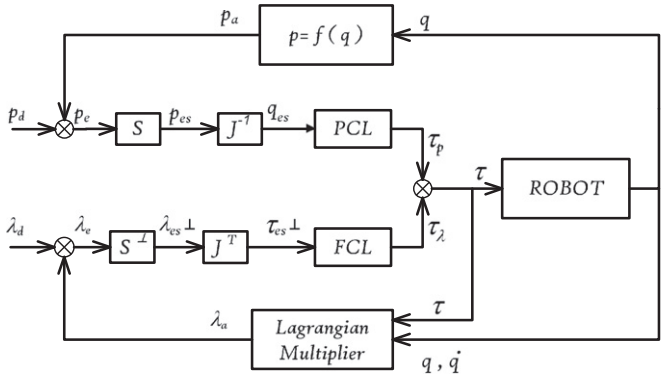

Fig. 4. Hybrid position/force controller.

where q_e is joint error and Eqs. (18) and (19) represent selected Cartesian error and selected joint error, respectively.

As shown in Fig. 4, using the selection matrices in the two control loops guarantees that the position and force control is decoupled. Therefore, the control law for each loop can be designed independently. Usually, a form of *PID* controller is adequate for position control, while other schemes such as computed torque control can also be applied to enhance control performance by including the dynamics of the manipulator in the controller. In the force control loop, a force-based explicit control can be used. If the force sensor signal is noisy, *PI* controller can be used in the control law to alleviate the noise effect. The control command is thus given by

$$\tau = \tau_p + \tau_\lambda$$

where τ_p corresponds to the command torques to minimize the position error P_e and τ_λ corresponds to the command torques to minimize force error λ_e as follows:

$$\tau_p = K_{pp}(p_d - p_a) + K_{dp}(\dot{p}_d - \dot{p}_a) + K_{ip}\int_0^t (p_d - p_a)\, d\tau$$

$$\tau_\lambda = K_{pf}(\lambda_d - \lambda_a) + K_{if}\int_0^t (\lambda_d - \lambda_a)\, d\tau \tag{21}$$

The required conditions for kinematic stability of the control scheme expressed in the joint space are

$$q_e^T (SJ)^{\dagger}(SJ) q_{es} \geq 0, \quad q_e^T [I - (SJ)^{\dagger}(SJ)] q_{es} \geq 0 \tag{22}$$

$$\|q_{es}\| \leq \|q_e\| \tag{23}$$

The first set of inequality conditions guarantees that the orthogonal components of the q_{es} projection are in the same direction as those of q_e which avoids positive feedback from occurring in the position loop, while the second condition guarantees that the norm of the vector of the selected joint errors is bounded when the norm of the joint error vector is bounded. It is shown in [21] that the original hybrid control scheme does not satisfy the first set of conditions, which implies that kinematic instability can occur in the original control scheme.

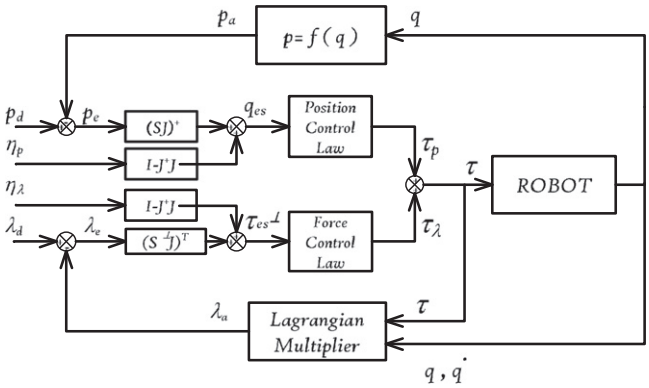

Fig. 5. Modified hybrid position/force controller.

It is shown in [22,21] that the kinematic instability problem arises in manipulators with revolute joints due to the inappropriate formulation of selected joint space variables in the position control loop. More specifically, using the inverse of the Jacobian matrix to map the selected position error to the selected joint error causes this phenomena. In [22], the linearized closed-loop system of the original hybrid position/force control is used to show the instability in the position control loop. In this section, we explain why Eq. (19) is not a valid formulation and propose a solution to resolve the problem. A modified hybrid control scheme proposed in [21] is used in this study as depicted in Fig. 5, showing that the extra terms corresponding to the null space of J are added to the minimum norm solutions in both loops.

Thus

$$q_{es} = (SJ)^{\dagger} p_e + [I - J^{\dagger} J]\eta_p \tag{24}$$

$$\tau_{es} = (S^{\perp} J)^T \lambda_e + [I - J^{\dagger} J]\eta_\lambda \tag{25}$$

where, η_p and η_f are any arbitrary vectors belonging to the joint space such that the stability conditions previously discussed are satisfied. One stable candidate is $\eta_p = 0$ and $\eta_f = 0$ [21].

4. Experimental setup and results

Before presenting the experimental results, first let us briefly describe the experimental setup. Joint angles are obtained using digital magneto-resistance encoders with a physical resolution of 1024 pulses per revolution attached to the motors. Joint velocities are calculated using a stable high gain observer. Also, the deflection of the flexible beam is required along with the exerted normal force to the environment. A six-axis high resolution force/torque sensor is used for the above purpose. The force sensor is attached to the rigid linkage using a detachable jaw designed to hold either a needle or a flexible beam as shown in Fig. 6.

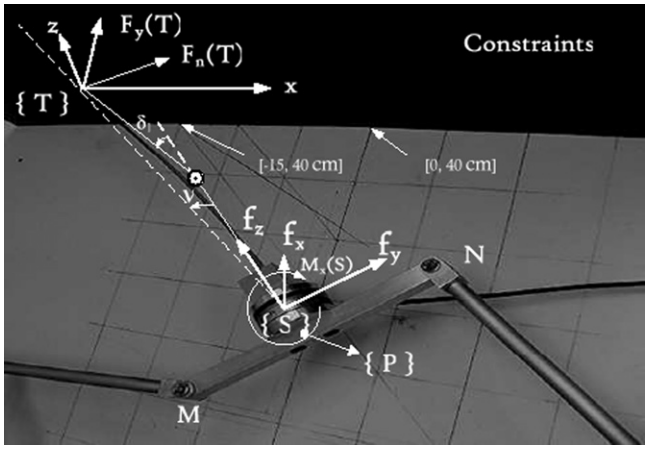

Fig. 6. Coordinate definitions for the flexible manipulator sliding along the rigid environment.

To estimate the deflection of the flexible beam and the force value normal to the environment we use an approximation in the static case as follows:

$$F_n(T) = \frac{M_x(S)}{L_f} = \frac{3EI_z}{L_f^2}\upsilon \tag{26}$$

$$\upsilon = \frac{M_x(S)L_f}{3EI_z} \tag{27}$$

where $F_n(T)$ is the force at point T normal to the end of the flexible beam, $M_x(S)$ represents the bending moment measured about the x-axis of the force sensor, υ denotes the deflection angle, and $I_z = HW^3/12$ is the moment of inertia of the flexible beam. H and W are height and width of the flexible beam, respectively. As shown in Fig. 6, the flexible beam is modeled using two equal rigid sub-links connected by a spring. Thus, we have

$$\delta_1 = 2\upsilon \tag{28}$$

Experiments were conducted to verify if the estimated values of deflection given by Eqs. (26)–(28) match the real values. The results show that if the deflection is less that 20% of the link length, the approximations are close to the real values.

Now, given the deflection angle of the deflected flexible beam, the normal force on the environment can be calculated using force transformation as follows:

$${}^{T}\mathrm{F}_{T} = {}^{T}_{S}\mathrm{T}_{f}\,{}^{S}\mathrm{F}_{S}$$

where, ${}^{T}\mathrm{F}_{T}$, ${}^{T}_{S}\mathrm{T}_{f}$, and ${}^{S}\mathrm{F}_{S}$ are the force sensor measurements with respect to frame T, the transformation matrix, and the force measurements with respect to the sensor frame, respectively. The transformation matrix is given by

$${}^{T}_{S}\mathrm{T}_{F} = \begin{bmatrix} {}^{T}_{S}\mathrm{R} & 0 \\ {}^{T}\mathrm{P}_{sorg} \times {}^{T}_{S}\mathrm{R} & {}^{T}_{S}\mathrm{R} \end{bmatrix} \tag{29}$$

where

$$ {}^{S}_{T}\mathrm{R} = R_Y(90^\circ)\cdot R_Z(\delta)\cdot R_Z(\varphi-\pi) \tag{30} $$

$$ \varphi = \zeta-\delta_1 \tag{31} $$

As a result, the measured forces with respect to frame T are given by

$$ F_y\{T\} = \cos(\varphi)\sin(\delta_1)f_x + \cos(\varphi)\cos(\delta_1)f_y + \sin(\varphi)f_z \tag{32} $$

where f_x, f_y, and f_z are the three force elements of the force sensor along its coordinate axis, respectively. This estimation was verified experimentally by locating another force sensor on the environment to measure the actual force sensed by the environment. The beam length is 29 cm with a Young's modulus of elasticity $E=20\times10^{10}$, mass of 20 g and dimensions 0.72 mm × 10 mm.

The data from the encoders and the force sensor are sent to a data acquisition system. Data are acquired and processed under the XPC-Target environment in MATLAB® and the command signals are sent to the actuators using PWM amplifiers. It is important to note that throughout all the experiments, a constant time step of 2 ms was used in the data acquisition and controller implementation.

Figs. 7 and 8 show the desired and actual forces exerted on the environment and the position along the X-axis. The end point position is obtained from the measured joint angles and elastic displacements. The small errors in force (0.02 N) and position (0.3 mm) are due to the un-modeled friction force between the tool and the environment. In the experimental results shown in Figs. 9 and 10, a two-times faster trajectory has been used for the position profile. The results show that the tracking errors in both position and force control loops are very small but larger than the results in Figs. 7 and 8. In Fig. 11, the deflection mode of the flexible beam within the course of moving and applying force is shown. As expected, no deflection occurs when the desired force is zero, and the deflection increases as the desired force increases.

Two experiments were designed to investigate the robustness of the controller and the effect of the environment's deformability on the controller. In the first experiment, whose results are shown in Figs. 12 and 13, a surgical blade is fixed at the tip of the flexible beam and the rigid environment is replaced by a deformable environment with a uniform

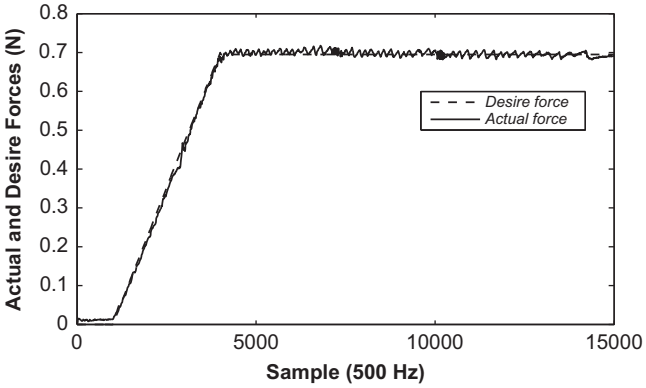

Fig. 7. Actual and desired forces (N) for a 30 s position trajectory.

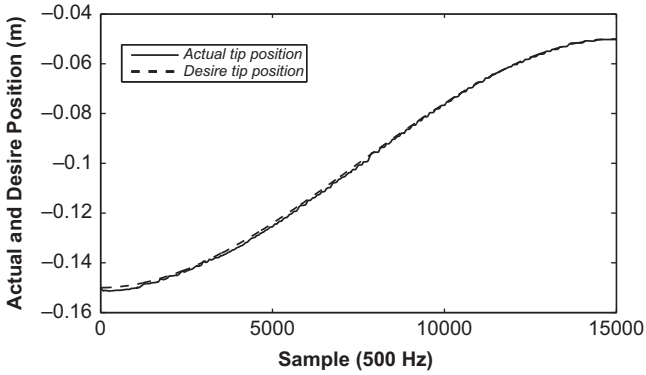

Fig. 8. Actual and desired tip positions within 30 s trajectory (m).

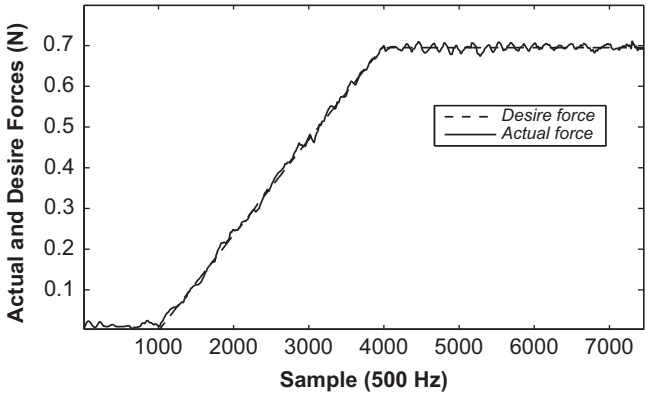

Fig. 9. Actual and desired forces (N) for a 15 s position trajectory.

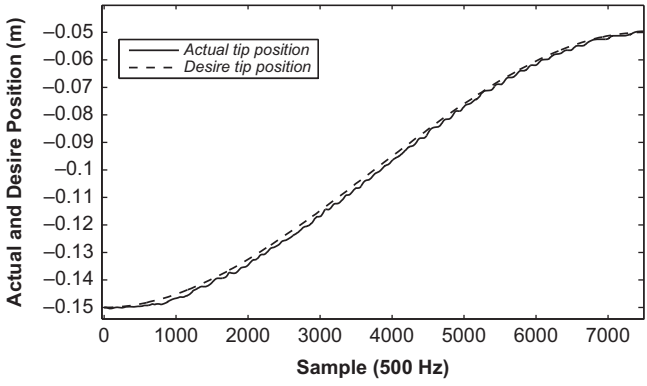

Fig. 10. Actual and desired tip positions for a 15 s trajectory (m).

elasticity, while in the second experiment, the environment consists of a soft environment located on a more deformable object. The objective of both experiments is cutting the environment and investigating the performance and robustness of the controller. The first

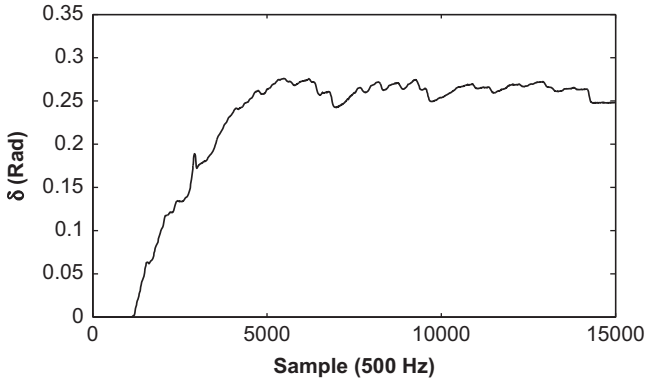

Fig. 11. Deflection mode of the flexible link (Rad).

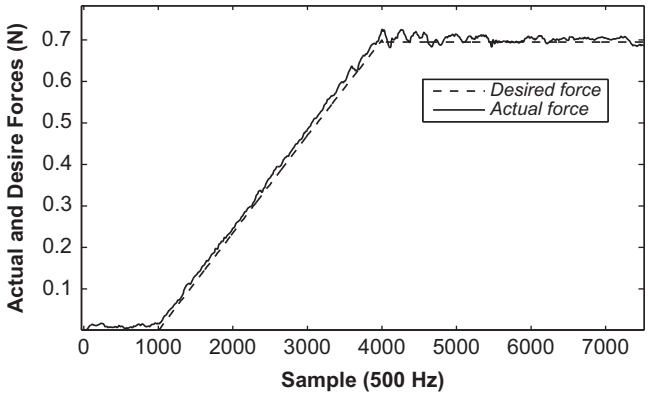

Fig. 12. Actual and desired forces (N) for a 15 s position trajectory when environment is deformable.

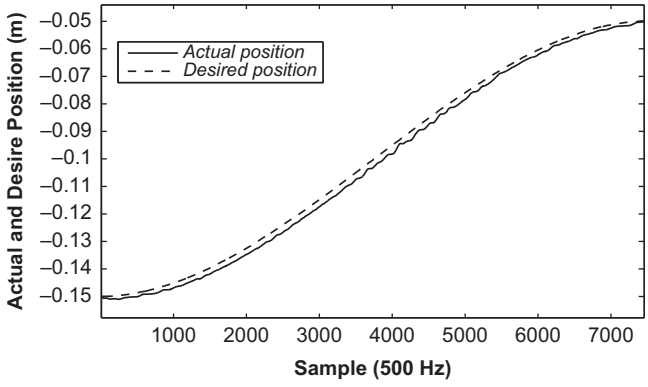

Fig. 13. Actual and desired tip positions for a 15 s trajectory (m) when environment is deformable.

experiment showed that the maximum error in the position (1.1 mm) and force (0.04 N) is relatively small but bigger than those for the rigid environment. Also, compared to the previous cases, there is more error in the position profile. This is due to the fact that

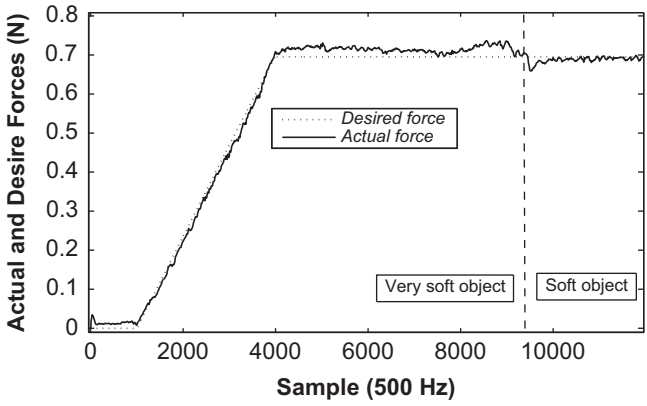

Fig. 14. Actual and desired forces (N) for a 24 s position trajectory when the elasticity of the environment is not uniform.

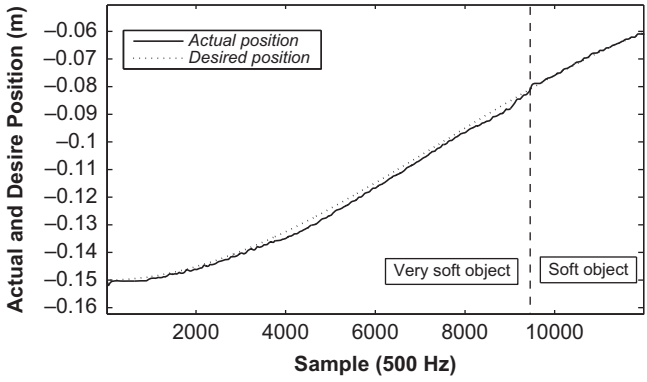

Fig. 15. Actual and desired tip positions for a 24 s trajectory (m) when the elasticity of the environment is not uniform.

penetration of the blade inside the environment during the experiment causes a position error in Y-direction which is neglected in the position loop control law (Eq. (21)) through the selection matrix S. Figs. 14 and 15 show the results of the second experiment. Also, some of the errors observed in the position and force are due to the frictional forces involved in the cutting procedure. The system behaves in a robust manner and is stable despite the fact that the flexibility of the deformable environment was not modeled in the controller.

5. Conclusion

This paper deal with position/force control of a flexible manipulator designed as a test bed to investigate simultaneous position and force control. In this regard, a modified hybrid position/force control scheme was implemented and the results were compared when slow and fast position profiles were used. The results indicate small errors in position and force which increase for faster position trajectories. The experiments were also

conducted for contact with deformable environments. Although, the errors in position and force were quite small, it was observed that as the desired force or the elasticity of the environment is increased, larger errors in position were obtained as a result of higher position errors in the force-controlled direction.

References

[1] H. Sadjadi, M.A. Jarrah, Autonomous cleaning system for Dubai international airport, Journal of the Franklin Institute 348 (1) (2011) 112–124.
[2] G. Dogangil, B.L. Davies, F. Rodriguez, Y. Baena1, A review of medical robotics for minimally invasive soft tissue surgery, Proceedings of the Institute of Mechanical Engineers, Part H: Journal of Engineering in Medicine 224 (5) (2010) 653–679.
[3] S. Ito, H. Kawasaki, Y. Ishigure, M. Natsume, T. Mouri, Y. Nishimoto, A design of fine motion assist equipment for disabled hand in robotic rehabilitation system, Journal of the Franklin Institute 348 (1) (2011) 79–89.
[4] R. Alterovitz, K. Goldberg, J. Pouliot, R. Taschereau, I.C. Hsu, Needle insertion and radioactive seed implantation in human tissues: simulation and sensitivity analysis, in: IEEE International Conference on Robotics and Automation, Taipei, Taiwan, 2003, pp. 1793–1799.
[5] P. DiMaio, S. E. Salcudean, Needle insertion modeling and simulation, in: IEEE International Conference on Robotics and Automation, Washington DC, 2002, pp. 2099–2105.
[6] R.H. Cannon, E. Schmitz, Initial experiments on the endpoint control of a flexible one-link robot, International Journal of Robotics Research 3 (3) (1984) 62–75.
[7] K. Cho, N. Hori, J. Angeles, On the controllability and observability of flexible beams under rigid-body motion, in: International Conference on Industrial Electronics, Control and Instrumentation, Kobe, Japan, 1991, pp. 455–460.
[8] T. Yoshikawa, K. Hosoda, Modeling of flexible manipulators using virtual rigid links and passive joints, International Journal of Robotics Research 15 (1996) 290–299.
[9] O.A. Bauchau, Parallel computation approaches for flexible multibody dynamics simulations, Journal of the Franklin Institute 347 (1) (2010) 53–68.
[10] H. Krishnan, Design of force/position control laws for constrained robots, including effects of joint flexibility and actuator dynamics, Robotica 17 (1999) 41–48.
[11] G. Liu, Z. Li, A unified geometric approach to modeling and control of constrained mechanical systems, IEEE Transactions on Robotics and Automation 18 (4) (2002) 574–587.
[12] A. Bazaei, M. Moallem, Force transmission through a structurally flexible beam: dynamic modeling and feedback control, IEEE Transactions on Control Systems and Technology 17 (5) (2009) 1245–1256.
[13] A. Bazaei, M. Moallem, Control bandwidth improvement in force control of flexible-link arms by output redefinition, IEEE/ASME Transactions on Mechatronics 99 (2010) 1–7.
[14] F.O. Tellez, A.G. Loukianov, E.N. Sanchez, E.J.B. Corrochano, Decentralized neural identification and control for uncertain nonlinear systems: application to planar robot, Journal of the Franklin Institute 347 (6) (2010) 1015–1034.
[15] Y-H. Chen, X. Zhang, Adaptive robust approximate constraint-following control for mechanical systems, Journal of the Franklin Institute 347 (1) (2010) 69–86.
[16] C. Gosselin, J. Angeles, Singularity analysis of closed-loop kinematic chains, IEEE Transactions on Robotics and Automation 6 (3) (1994) 281–290.
[17] L. Stocco, S.E. Salcudean, F. Sassani, Fast constrained global minimax optimization of robot parameters, Robotica 16 (1998) 595–605.
[18] A.S. Zaki, W.H. El Maraghy, Modeling and control of two-link flexible manipulator, Journal of the Canadian Society of Mechanical Engineers 16 (1992) 311–328.
[19] R. Murray, Z.X. Li, S. Sastry, A Mathematical Introduction to Robotic Manipulation, CRC Press, Boca Raton, FL, 1994.
[20] J.J. Craig, Introduction to Robotics: Mechanics and Control, Addison-Wisley, London, 1989.
[21] W.D. Fisher, M.S. Mujtaba, Hybrid position/force control: a correct formulation, International Journal of Robotics Research 11 (4) (1992) 299–311.
[22] C.H. An, J.M. Hollerbach, Kinematic stability issue in force control of manipulators, in: IEEE International Conference on Robotics and Automation, Raleigh, NC, 1987, pp. 897–903.